On the magnetic structure of $PrMn_2O_5$: a neutron diffraction study

2012 J. Phys.: Condens. Matter 24 076003

(http://iopscience.iop.org/0953-8984/24/7/076003)

J. Phys.: Condens. Matter **24** (2012) 076003 (9pp) doi:10.1088/0953-8984/24/7/076003

On the magnetic structure of $PrMn_2O_5$: a neutron diffraction study

A Muñoz[1], J A Alonso[2], M J Martínez-Lope[2], V Pomjakushin[3] and G André[4]

[1] Departamento Física Aplicada, EPS, Universidad Carlos III, Avenida Universidad, 30, Leganés-Madrid, E-28911, Spain
[2] Instituto de Ciencia de Materiales de Madrid, CSIC, Cantoblanco, E-28049 Madrid, Spain
[3] Laboratory for Neutron Scattering, ETH Zurich & PSI Villigen, CH-5232, Villigen, Switzerland
[4] Laboratoire Leon Brillouin, CEA Saclay, F-9119 Gif sur Ivette, France

E-mail: angel.munoz@uc3m.es

Received 29 August 2011, in final form 20 December 2011
Published 18 January 2012
Online at stacks.iop.org/JPhysCM/24/076003

Abstract

The long-range magnetic ordering of $PrMn_2O_5$ has been studied on polycrystalline samples from neutron diffraction and specific heat measurements. The onset of antiferromagnetic ordering is observed at $T_N \approx 25$ K. In the temperature interval 18 K $< T <$ 25 K the magnetic structure is defined by the propagation vector $\mathbf{k}_1 = (1/2, 0, 0)$. Below 18 K, some additional magnetic satellites appear in the NPD patterns, which are indexed with $\mathbf{k}_2 = (0, 0, 1/2)$. Therefore, below 18 K the magnetic structure consists of two independent magnetic domains, defined by the propagation vectors $\mathbf{k}_1$ and $\mathbf{k}_2$. The magnetic structure of the $\mathbf{k}_1$-domain is given by the basis vectors $(C_x, 0, 0)$ and $(C'_x, 0, 0)$ for Mn(4h) and Mn(4f), respectively. In the $\mathbf{k}_2$-domain, the magnetic structure is defined by the basis vectors $(0, 0, G_z)$ and $(F'_x, G'_y, 0)$ for Mn(4h) and Mn(4f), respectively. At $T = 1.5$ K, for the magnetic phase associated with $\mathbf{k}_1$, the magnetic moments of the Mn atoms at the 4h and 4f sites are 1.82(7) and 1.81(6) μ_B, respectively; for the magnetic phase associated with $\mathbf{k}_2$, the magnetic moments for the Mn(4h) and Mn(4f) atoms are 0.59(5) and 2.62(5) μ_B, respectively.

(Some figures may appear in colour only in the online journal)

1. Introduction

The observation of a strong correlation between magnetic ordering and ferroelectricity in some members of the oxide family RMn_2O_5 (R = rare earth, Y and Bi), such as $TbMn_2O_5$ [1], $DyMn_2O_5$ [2] and $HoMn_2O_5$ [3], has revived the interest in these materials, since they are among the few compounds where the application of an external magnetic field can control the electrical polarization. The first studies concerning the crystallographic structure of RMn_2O_5 oxides were carried out by Quezel-Ambrunaz *et al* [4] and Bertaut *et al* [5] in the 1960s. In these pioneering works the main features of the crystallographic structures were established. They are orthorhombic, space group *Pbam*; in the unit cell there are two distinct positions for the Mn ions that present different oxidation states, Mn^{4+} at 4f and Mn^{3+} at 4h Wyckoff sites. The Mn^{4+} ions are octahedrally coordinated to oxygens, whereas each Mn^{3+} ion has five oxygen atoms as closer neighbors forming a tetragonal pyramid. The crystal structure is described as a set of $Mn^{4+}O_6$ edge-linked octahedra forming ribbons arranged along the *c* direction. Two $Mn^{3+}O_5$ tetragonal pyramids join together via a double Mn–O–Mn bond giving rise to a Mn_2O_{10} dimer. The different $Mn^{4+}O_6$ ribbons are connected by these dimers. A subsequent study of the crystallographic structure from high-resolution neutron diffraction data [6, 7] established that the sizes of the $Mn^{4+}O_6$ and $Mn^{3+}O_5$ polyhedra progressively decrease as the R^{3+} ionic radius becomes smaller.

The RMn_2O_5 compounds exhibit an antiferromagnetic ordering [8, 9] with an onset temperature T_N that, depending on the rare earth R^{3+} ion, is in the 30–45 K range. The magnetic structures of some members of the RMn_2O_5 series, such as R = Nd, Tb, Ho, Er and Y, were analyzed a long time ago from neutron diffraction experiments [10, 11]. The

first studies reported that below T_N the Mn^{3+} and Mn^{4+} ions present a magnetic structure defined by the propagation vector $\mathbf{k} = (1/2, 0, \tau)$, where τ varies depending on the rare earth. The spin arrangement for both Mn sublattices is given by a helicoidal structure with the moments in the *ab* plane. The R^{3+} cations become ordered at a lower temperature with a sinusoidal magnetic structure. These results were partially revisited for $ErMn_2O_5$ and $TbMn_2O_5$ [12]. In principle, it seemed that all the compounds of the RMn_2O_5 family would exhibit a magnetic structure with similar features, in all cases defined by $\mathbf{k} = (1/2, 0, \tau)$, but further studies have reported a certain diversity: some of the compounds such as $BiMn_2O_5$ [13, 14] and $LaMn_2O_5$ [15] show a commensurate magnetic structure defined by the propagation vectors $\mathbf{k} = (1/2, 0, 1/2)$ and $\mathbf{k} = (0, 0, 1/2)$, respectively. On the other hand, the magnetic order below T_N of other members of the RMn_2O_5 series, such as R = Y, Tb, Ho, is quite complex [16], with different magnetic transitions. The following sequence of magnetic transitions has been observed in these oxides: immediately below T_N the magnetic structure is incommensurate and defined by $\mathbf{k} = (k_x, 0, k_z)$; a few degrees below T_N a ferroelectric transition at T_C takes place and simultaneously a magnetic transition to a commensurate magnetic structure occurs, which is defined by the propagation vector $\mathbf{k} = (1/2, 0, 1/4)$; however, on decreasing the temperature a new magnetic transition to an incommensurate magnetic structure appears, and again the propagation vector is of the type $\mathbf{k} = (k_x, 0, k_z)$. For $DyMn_2O_5$ [16, 17] the sequence of magnetic transitions is similar, except that below 8 K new magnetic reflections associated with $\mathbf{k} = (1/2, 0, 0)$ are also observed.

In ferroelectric materials with a magnetic order, T_C usually appears in the paramagnetic region; conversely in RMn_2O_5 the ferroelectric order takes place in the magnetically ordered region [18, 19], the spontaneous polarization being established along the *b*-direction of the orthorhombic structure. Furthermore, the different magnetic transitions that are observed in the ordered region are also accompanied by anomalies both in the dielectric constant and in the polarization [20–23]. This observation highlights the great correlation that exists in these compounds between ferroelectricity and magnetic order. Therefore, in other to understand the origin of the interplay between ferroelectricity and magnetic order, it is of paramount importance to establish the magnetic phase diagram of the compounds of the RMn_2O_5 family.

The aim of this work is to analyze the magnetic structure of $PrMn_2O_5$ below the ordering temperature T_N, and study its evolution along the ordered region. Former contributions on the preparation of the R = La and Pr members of the RMn_2O_5 family indicated [6] that they must be synthesized under high oxygen pressure to favor the stabilization of Mn^{4+}, already establishing the main crystallographic features of $PrMn_2O_5$ and its macroscopic magnetic properties, reporting $T_N = 25$ K. The present study of the magnetic structure has been carried out from neutron diffraction measurements complemented with specific heat measurements.

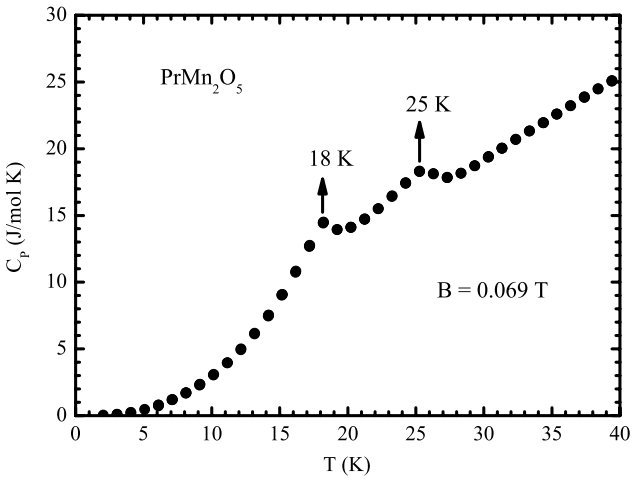

Figure 1. Thermal evolution of the specific heat in the temperature interval 2 K < T < 40 K.

2. Experimental details

$PrMn_2O_5$ was obtained as a dark brown polycrystalline powder starting from precursors previously synthesized by a wet-chemistry technique, followed by oxygenation at 1000 °C under 200 bar of oxygen pressure, as indicated elsewhere [6]. It is important to underline that the final treatment under high oxygen pressure is essential for the stabilization of monophased $PrMn_2O_5$. This material could not be obtained at ambient pressure starting either from citrate precursors or from ceramic mixtures since the competitive, very stable $PrMnO_{3+\delta}$ perovskite was always present in the final product.

The specific heat measurements were carried out in a semiadiabatic He calorimeter using the heat-pulsed method from 2 up to 40 K in a PPMS device. The neutron powder diffraction (NPD) patterns were acquired at the Orphée reactor (LLB-Saclay), at the G4-1 two-axis diffractometer. The NPD patterns were collected at different temperatures in 2 K steps and in the temperature interval 1.5 K < T < 25.7 K with a wavelength of 2.424 Å. The refinements of the crystallographic and the magnetic structures were performed by using the Rietveld method [24] with FULLPROF [25] software. In the profile refinements, the peak shape was simulated by a pseudo-Voigt function and the background was fitted with a fifth-degree polynomial function. The coherent scattering lengths used in the refinements for Pr, Mn and O were 4.58, −3.73 and 5.803 fm, respectively.

3. Results

3.1. Specific heat measurements

The specific heat measurements carried out under a weak magnetic field of 0.069 T are reported in figure 1. In the thermal evolution of the specific heat two anomalies are observed at 25 K and at 18 K. As will be shown in the NPD measurements, the first anomaly is related to the appearance of a magnetic order with $T_N \approx 25$ K. As regards the anomaly observed at 18 K, it is related to a change of the magnetic structure observed below T_N.

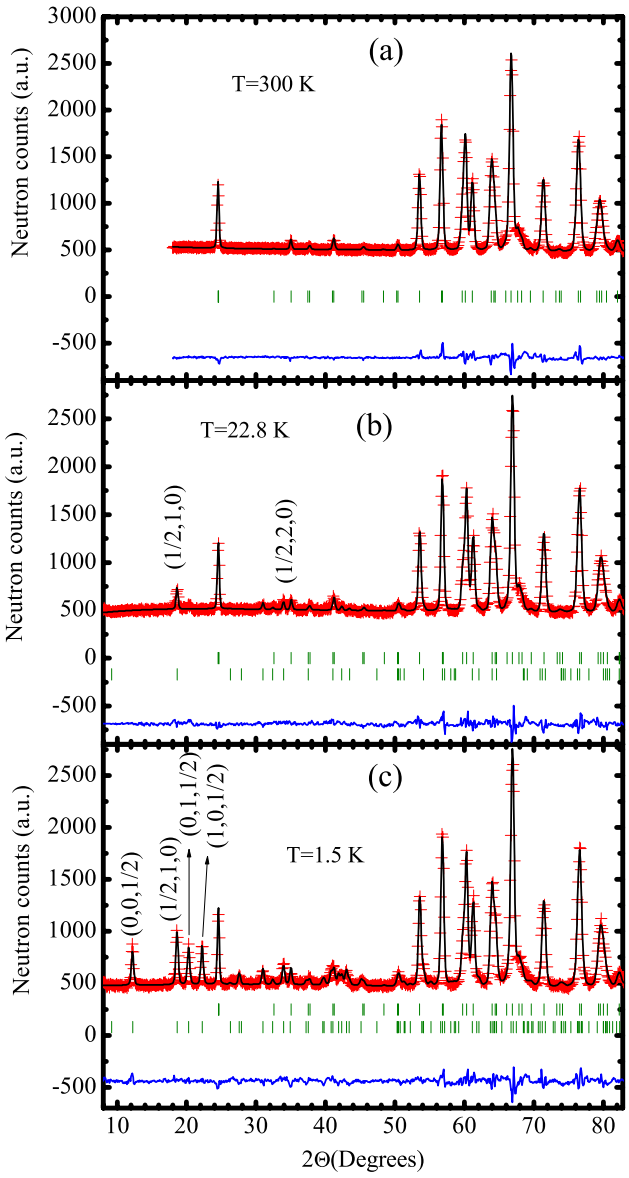

Figure 2. Observed (crosses) and calculated (solid line) NPD patterns at (a) 310 K, (b) 22.8 K and (c) 1.5 K. The first series of tick marks corresponds to the nuclear reflections and the second one to the magnetic satellites. The solid line at the bottom is the difference between the observed and calculated NPD patterns.

3.2. Neutron diffraction measurements

An NPD pattern acquired at 310 K was fitted by considering the crystallographic structure formerly given for $PrMn_2O_5$ [6]. All the Bragg reflection observed in the pattern could be indexed with the lattice parameters $a = 7.5622(6)$ Å, $b = 8.6485(6)$ Å and $c = 5.7154(5)$ Å, corresponding to an orthorhombic unit cell of the space group Pbam; a good agreement between the observed and calculated NPD profiles was reached, as shown in figure 2(a). A perspective of the crystal structure is displayed in figure 3.

On analyzing the thermal evolution of the NPD patterns, new peaks appear at around 25.7 K which are clearly seen at 22.8 K. This indicates the appearance of a magnetic order

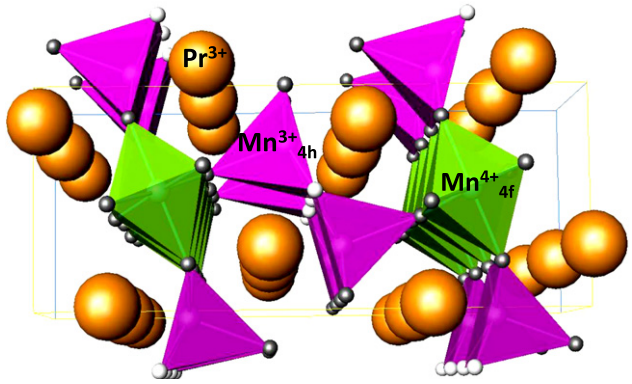

Figure 3. View of the $PrMn_2O_5$ crystal structure, highlighting the pyramidal coordination of Mn^{3+} at 4h sites and octahedral environment of Mn^{4+} at 4f positions. The MnO_6 octahedra share edges to form infinite chains along the c axis; the MnO_5 pyramids form dimer units that link the chains together.

in good agreement with the specific heat curve. These peaks can be indexed with the propagation vector $\mathbf{k}_1 = (1/2, 0, 0)$. On decreasing the temperature, new magnetic peaks appear below 18.8 K, but these new magnetic peaks are indexed with the propagation vector $\mathbf{k}_2 = (0, 0, 1/2)$. These results reveal that the magnetic structure of $PrMn_2O_5$ is given by $\mathbf{k}_1$ in the temperature interval 18 K $< T <$ 25 K and by the propagation vectors $\mathbf{k}_1$ and $\mathbf{k}_2$ for $T <$ 18 K. In figure 4 the thermal evolution of the magnetic reflections $(1/2, 1, 0)$ and $(0, 0, 1/2)$ is shown.

The possible magnetic structures compatible with the symmetry have been determined with the aid of the representation analysis technique described by Bertaut [26] by using the program BasIreps contained in the FULLPROF_Suite package [25]. The Mn atoms at the site 4h are denoted as $1(x, y, 1/2)$, $2(-x, -y, 1/2)$, $3(-x+1/2, y+1/2, -1/2)$ and $4(x + 1/2, -y + 1/2, -1/2)$. For the Mn atoms at the site 4f, the notation is $5(1/2, 0, z)$, $6(0, 1/2, -z)$, $7(-1/2, 0, -z)$ and $8(1, 1/2, z)$. For the propagation vector $\mathbf{k}_1 = (1/2, 0, 0)$, the small group $G_{\mathbf{k}1}$ has two bi-dimensional irreducible representations. As is shown in table 1, for both 4h and 4f sites, the four Mn atoms of the same site are subdivided into two orbits, which implies that the magnetic moments of the Mn atoms belonging to the same site can be different. However, on determining the magnetic order associated with the magnetic satellites of $\mathbf{k}_1 = (1/2, 0, 0)$, only those solutions giving rise to the same magnetic moment for all of the atoms of the same site have been considered. On the other hand, for $\mathbf{k}_2 = (0, 0, 1/2)$, the small group $G_{\mathbf{k}2}$ has eight mono-dimensional irreducible representations. In this case, as is shown in table 2, for both sites the Fourier components of the four Mn atoms of the same site are symmetry related.

After checking the different solutions, for the magnetic order associated with $\mathbf{k}_1 = (1/2, 0, 0)$, the best fitting of the intensities of the $\mathbf{k}_1$ magnetic satellites is obtained if the coupling of the corresponding Fourier components is given by the basis vectors $(C_x, 0, 0)$ and $(C'_x, 0, 0)$ for Mn(4h) and Mn(4f), respectively. For the magnetic order corresponding to $\mathbf{k}_2$ the best agreement is achieved if the structure is given

Table 1. Basis vectors determined for the propagation vector $\mathbf{k}_1 = (1/2, 0, 0)$ with respect to the space group Pbam.

	Mn(4h)				Mn(4f)			
	1	2	3	4	5	7	6	8
Γ^1	$\phi_{11}(0,0,1)$	$(0,0,1)$	$\phi_{13}(0,0,-1)$	$(0,0,1)$	$\psi_{11}(1,0,0)$	$(1,0,0)$	$\psi_{14}(-1,0,0)$	$(-1,0,0)$
	$\phi_{12}(0,0,1)$	$(0,0,-1)$	$\phi_{14}(0,0,-1)$	$(0,0,-1)$	$\psi_{12}(0,1,0)$	$(0,1,0)$	$\psi_{15}(0,1,0)$	$(0,1,0)$
					$\psi_{13}(0,0,1)$	$(0,0,-1)$	$\psi_{16}(0,0,-1)$	$(0,0,1)$
Γ^2	$\phi_{21}(1,0,0)$	$(-1,0,0)$	$\phi_{25}(-1,0,0)$	$(-1,0,0)$	$\psi_{21}(1,0,0)$	$(-1,0,0)$	$\psi_{24}(-1,0,0)$	$(1,0,0)$
	$\phi_{22}(0,1,0)$	$(0,-1,0)$	$\phi_{26}(0,1,0)$	$(0,1,0)$	$\psi_{22}(0,1,0)$	$(0,-1,0)$	$\psi_{25}(0,1,0)$	$(0,-1,0)$
	$\phi_{23}(1,0,0)$	$(1,0,0)$	$\phi_{27}(-1,0,0)$	$(1,0,0)$	$\psi_{23}(0,0,1)$	$(0,0,1)$	$\psi_{26}(0,0,-1)$	$(0,0,-1)$
	$\phi_{24}(0,1,0)$	$(0,1,0)$	$\phi_{28}(0,1,0)$	$(0,-1,0)$				

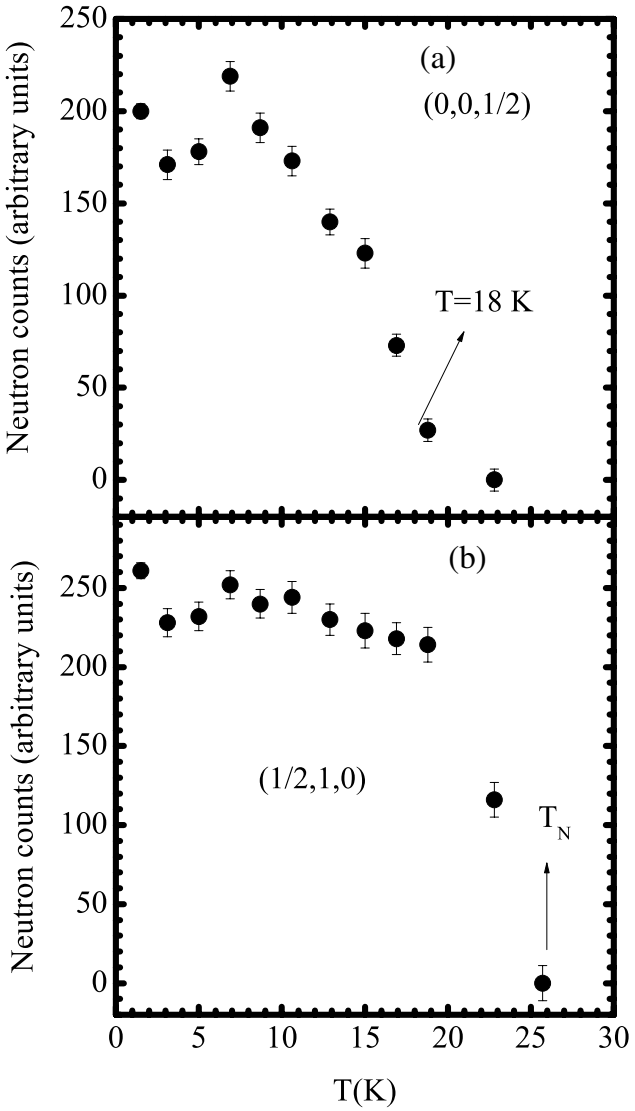

Figure 4. Thermal evolution of the integrated intensities of the magnetic reflections $(0, 0, 1/2)$ (a) and $(1/2, 1, 0)$ (b).

by the basis vectors $(0, 0, G_z)$ and $(F'_x, G'_y, 0)$ for Mn(4h) and Mn(4f), respectively. The values of the Fourier components obtained in the fitting at $T = 1.5$ K are reported in table 3. The good agreement between the observed and calculated patterns at $T = 22.8$ and 1.5 K can be appreciated in figures 2(b) and (c).

Table 2. Basis vectors determined for the propagation vector $\mathbf{k}_2 = (0, 0, 1/2)$ with respect to the space group Pbam.

	Mn(4h)	Mn(4f)
Γ^1	$(A_x, G_y, 0)$	$(0, 0, G'_z)$
Γ^2	$(0, 0, C_z)$	$(0, 0, A'_z)$
Γ^3	$(G_x, A_y, 0)$	$(0, 0, F'_z)$
Γ^4	$(0, 0, F_z)$	$(0, 0, C'_z)$
Γ^5	$(0, 0, A_z)$	$(G'_x, F'_y, 0)$
Γ^6	$(C_x, F_y, 0)$	$(A'_x, C'_y, 0)$
Γ^7	$(0, 0, G_z)$	$(F'_x, G'_y, 0)$
Γ^8	$(F_x, C_y, 0)$	$(C'_x, A'_y, 0)$

$F = m_1 + m_2 + m_3 + m_4$
$G = m_1 - m_2 + m_3 - m_4$
$C = m_1 + m_2 - m_3 - m_4$
$A = m_1 - m_2 - m_3 + m_4$
$F' = m_5 + m_6 + m_7 + m_8$
$G' = m_5 - m_6 + m_7 - m_8$
$C' = m_5 + m_6 - m_7 - m_8$
$A' = m_5 - m_6 - m_7 + m_8$

On the one hand, let us point out that the propagation vectors $\mathbf{k}_1$ and $\mathbf{k}_2$ are not arms of the same **k**-star, as $\mathbf{k}_1$ and $\mathbf{k}_2$ are not related by the symmetry elements of the space group *Pbam*. On the other hand, as regards the magnetic structure of $PrMn_2O_5$ below 18 K, and in spite of $\mathbf{k}_1$ and $\mathbf{k}_2$ not belonging to the same **k**-star, two possibilities can be taken into consideration as concerns the magnetic structure of $PrMn_2O_5$ below 18 K. The first possibility would be a combination of $\mathbf{k}_1$ and $\mathbf{k}_2$ so that the magnetic structure has a single domain with a double **k**-structure. In the second case, both propagation vectors would be independent, each of them would correspond to a single **k**-structure and there would be two different magnetic domains in the magnetic structure of $PrMn_2O_5$.

In the case where the magnetic structure is a double **k**-structure, the total magnetic moment of the Mn atoms in each site is obtained on adding the associated magnetic moments obtained for each propagation vector $\mathbf{k}_i$. Only if the magnetic moments associated with $\mathbf{k}_1$ and $\mathbf{k}_2$ are perpendicular to each other does this solution lead to a magnetic structure with equal magnetic moments for all of the atoms of the same site. According to table 3, this would happen for the site 4h but not for the site 4f; therefore in this last case the magnetic moments of the Mn atoms would be different. Besides, the oxidation state of the Mn atoms at the

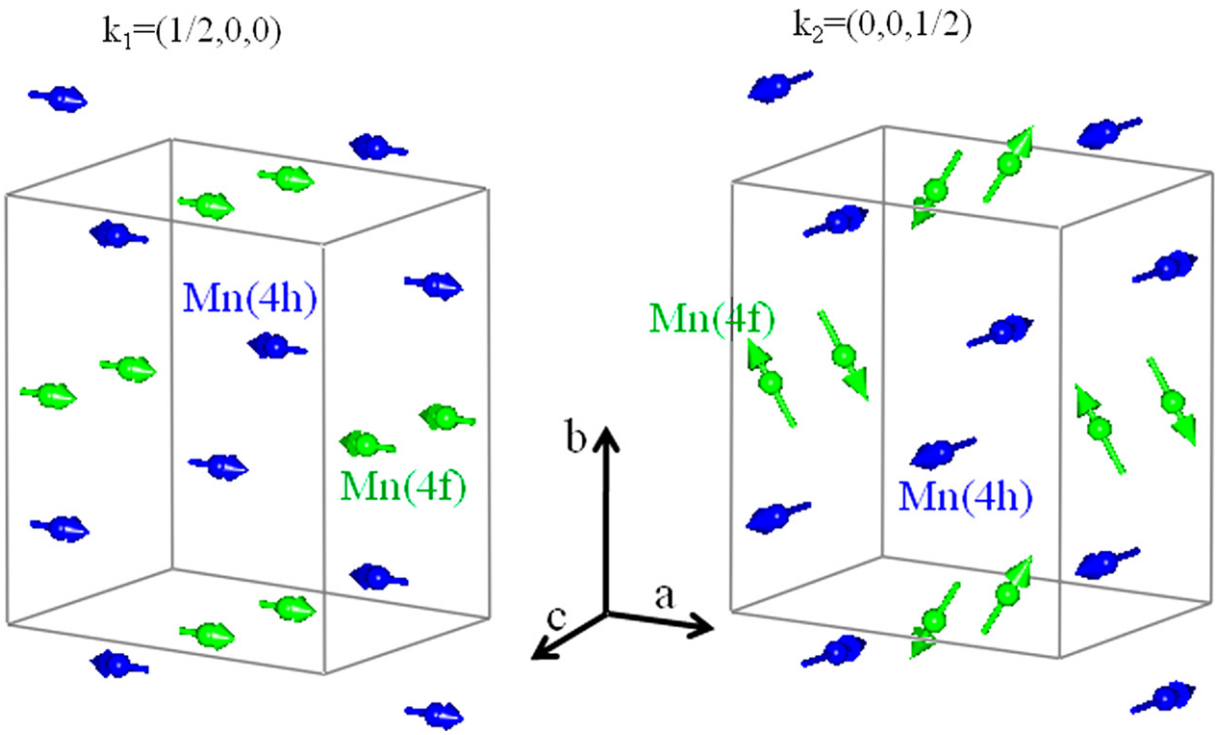

Figure 5. A view of the magnetic structures associated with the propagation vectors $\mathbf{k}_1 = (1/2, 0, 0)$ (magnetic phase 1) and $\mathbf{k}_2 = (0, 0, 1/2)$ (magnetic phase 2).

Table 3. Results from the magnetic structure refinement at $T = 1.5$ K.

	Mn(4h)		Mn(4f)
	$\mathbf{k}_1 = (1/2, 0, 0)$		
Solution	$(C_x, 0, 0)$		$(C'_x, 0, 0)$
S_x, S_y, S_z (μ_B)	1.82(7), 0, 0		1.82(6), 0, 0
	$\mathbf{k}_2 = (0, 0, 1/2)$		
Solution	$(0, 0, G_z)$		$(F'_x, G'_y, 0)$
S_x, S_y, S_z (μ_B)	0, 0, 0.59(5)		1.47(3), 2.17(4), 0
Discrepancy factors	R_B (Nuclear) = 3.3	R_B (Magnetic) = 11.8	$\chi^2 = 2.8$

4f site is $Mn^{4+}$and its electronic configuration is $t_{2g}^3 e_g^0$, with an expected magnetic moment of 3 μ_B per atom. According to table 3, on combining the magnetic moments of $\mathbf{k}_1$ and $\mathbf{k}_2$, the net magnetic moment for some of the Mn(4f) atoms would be around 4 μ_B, which is unphysically high. Therefore, these results indicate that below 18 K there would be two magnetic phases in $PrMn_2O_5$. One of them would be defined by the propagation vector $\mathbf{k}_1$ and the other one by $\mathbf{k}_2$. A plot of the magnetic structures of both magnetic phases is presented in figure 5. The thermal evolution of the magnetic moments of both magnetic phases is presented in figures 6 and 7.

Let us point out that the order of the Pr^{3+} sublattice has also been considered. However, the magnetic moment obtained from the fitting for the Pr atoms is always below 0.5 μ_B, so it has been considered that the Pr^{3+} sublattice is not magnetically ordered.

Another possibility has also been considered in the analysis of the magnetic structure of $PrMn_2O_5$. This solution consisted of assuming that each of the Mn sites becomes ordered according to the magnetic structure defined by only one of the propagation vectors below 18 K. On checking this possibility for $\mathbf{k}_2 = (0, 0, 1/2)$, it resulted that it was not possible to find a solution either for Mn(4h) or for Mn(4f) if the magnetic structure was given by the basis vectors belonging to only one of the irreducible representations shown in table 2. Therefore a mixture of basis vectors belonging to different propagation vectors was considered. In this case the best solutions imply that the magnetic ordering of Mn(4f) is given by the propagation vector $\mathbf{k}_2 = (0, 0, 1/2)$ and the magnetic structure of Mn(4h) by $\mathbf{k}_1 = (1/2, 0, 0)$. Two solutions were found: (i) (F'_x, G'_y, G'_z) for Mn(4f) $(\Gamma^1 + \Gamma^7)$ and $(F_x, 0, 0)$ for Mn(4h) and (ii) (A'_x, C'_y, G'_z) for Mn(4f) $(\Gamma^1 + \Gamma^6)$ and $(F_x, 0, 0)$ for Mn(4h). In both cases the magnetic discrepancy factor R_{mag} was above 20%. These possibilities were, therefore, discarded.

Let us point out that it is not usual to find a magnetic structure defined by two propagation vectors, as seems to be the case for $PrMn_2O_5$. However, there

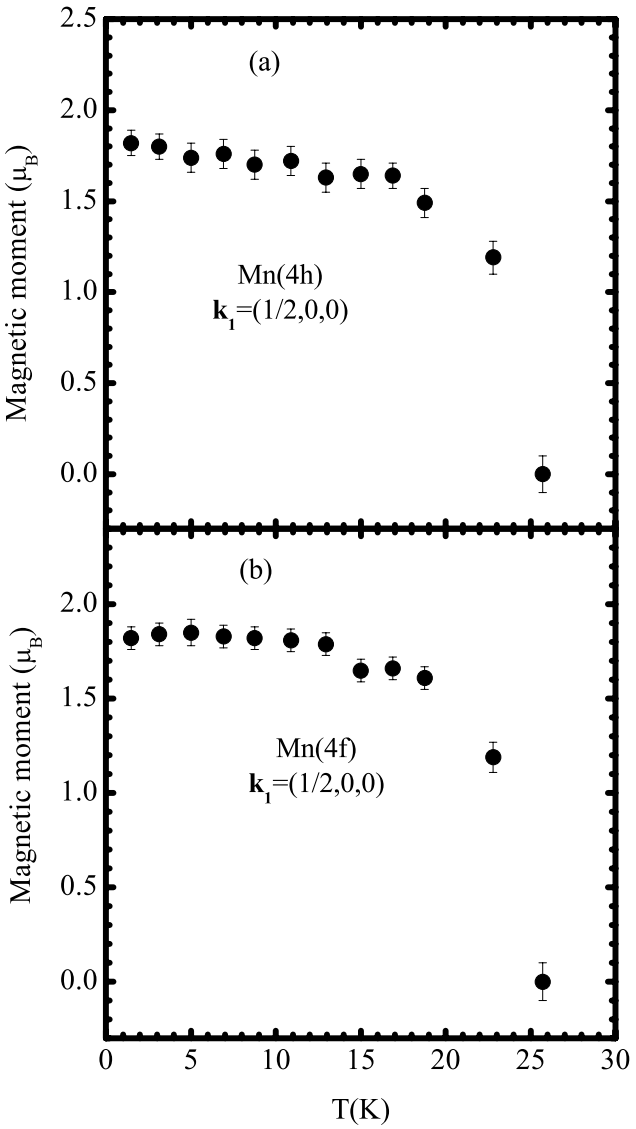

Figure 6. Thermal evolution of the magnetic moments of the Mn atoms at the sites 4h (a) and 4f (b). They correspond to the propagation vector $\mathbf{k}_1 = (1/2, 0, 0)$.

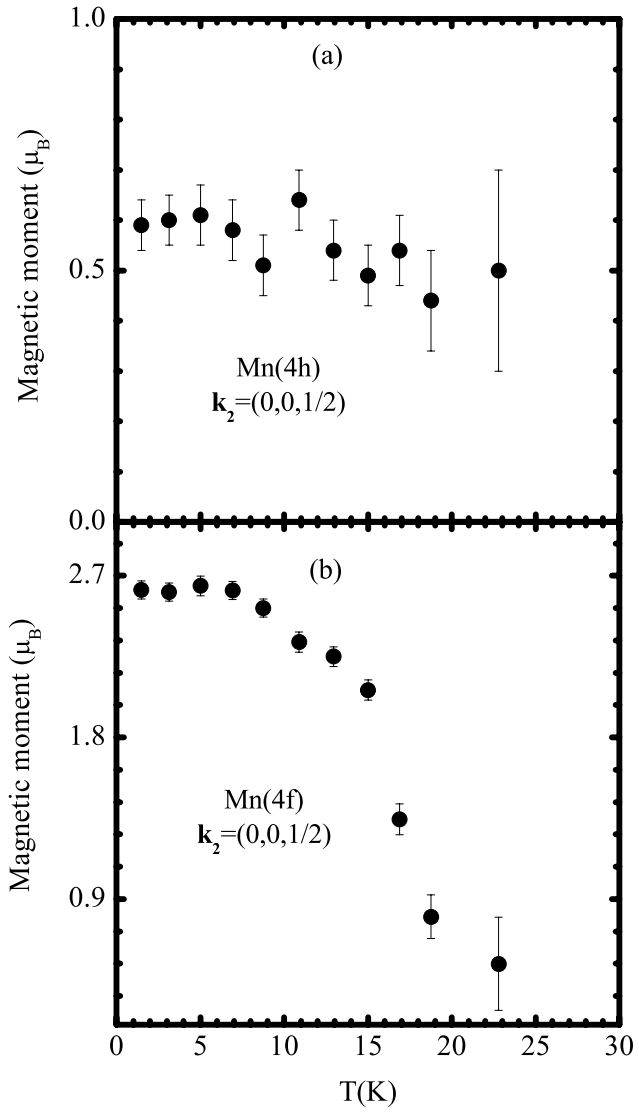

Figure 7. Thermal evolution of the magnetic moments of the Mn atoms at the sites 4h (a) and 4f (b). They correspond to the propagation vector $\mathbf{k}_2 = (0, 0, 1/2)$.

are an important number of compounds that also order according to a magnetic structure defined by several propagation vectors, such as $CeNi_{0.84}Sn_2$ [27], Ho_5Si_3 and Ho_5Ge_3 [28], $NdNi_{1-x}Cu_x$ [29], $U_2(Ni_{0.7}Pd_{0.3})_2Sn$ [30] or $FeNb_2O_6$, $NiNb_2O_6$ [31] or NaLMnWO$_6$ perovskites (L = La, Nd, Tb) [32]. $FeNb_2O_6$ and $NiNb_2O_6$ [31] seem to present a similar behavior to $PrMn_2O_5$, as there are two magnetic domains and the magnetic order in each domain is given by a different propagation vector. This implies that the magnetic energy is minimum in both cases, which is unexpected, unless the sample presents a phase separation effect. This phase separation may be associated with the presence of inhomogeneities, due to local strains or defects. This seems to be the case for $FeNb_2O_6$ and $NiNb_2O_6$ [31]. In the present case we have carried out an analysis of the profile width parameters for $PrMn_2O_5$ in order to explore the existence of some local strains that may explain the possible existence of a phase separation.

3.3. Analysis of the residual stress

The Rietveld method allows measurement of the influence of the crystallite size and the residual stress on the broadening of the Bragg reflections [33]. In the FULLPROF_Suite package [25], the microstructural effects are considered with a Voigt approximation. Both the instrumental and sample contributions to the profile are described by a convolution of a Lorentzian and a Gaussian function. If the sample does not show any microstructural effects, the dependence on the scattering angle θ of the full-width at half-maximum (denoted by H) of the Bragg peaks is given by the empirical Caglioti [34] formula:

$$H^2 = U_0 \tan^2\theta + V_0 \tan\theta + W_0 \qquad (1)$$

where U_0, V_0 and W_0 are refinable parameters characteristic of the diffractometer. In the case where the contribution of the size parameter follows the Debye–Scherrer formula and

Table 4. Crystallite size and microstrains in $PrMn_2O_5$.

Refined parameters	Size (Å)	Maximum strain (%)	R_B (%)	χ^2
U, I_G	569.7(2)	0.116 99(12)	6.7	1.4
U	—	0.220 4(1)	6.7	1.6
X	—	0.136 1(1)	4.9	1.3
X, I_G	844.8(5)	0.094 14(7)	5.3	1.3

the contribution of the strain parameter is proportional to $\tan(\theta)$, the dependences of the Lorentzian and Gaussian parts of the total full-width at half-maximum (convolution of the instrumental and intrinsic sample contributions to the profile) are written as

$$H_G^2 = U\tan^2\theta + V_0\tan\theta + W_0 + I_G/\cos^2\theta \quad (2)$$

$$H_L^2 = X\tan\theta + Y/\cos\theta \quad (3)$$

where V_0 and W_0 refer to the instrumental profile. U and X (I_G and Y) are the Gaussian and Lorentzian contributions of the strains (size) to the profile, respectively. Expressions (2) and (3) correspond to the isotropic model for describing the size–strain contribution to the broadening of the peak profile given by Fullprof.

The analysis of the residual stress was carried out on an NPD pattern acquired at $T = 25.7$ K. The parameters corresponding to the instrumental profile for the G4.1 instrument are $U_0 = 0.821$, $V_0 = -0.237$ and $W_0 = 0.078$. A preliminary refinement was carried out without any restriction on the parameters U, I_G, and Y; however, the refinement was not stable. Therefore, as indicated in table 4, different refinements were performed in which different parameters were refined. According to the data shown in table 4, in all cases the residual stress is very similar. In the case that the parameters X and I_G are refined, the apparent residual stress is 0.0941(7)% and the apparent crystallite size is 844.8(5) Å. This is within the order of magnitude observed in other samples with microstrain, for instance 0.12% in $LiCoO_2$ [35] or 0.34% in nanostructured Fe [36]. Therefore, according to this analysis it can be concluded that there exists a certain residual stress in our $PrMn_2O_5$ specimen.

4. Discussion

The specific heat and neutron diffraction measurements have shown that $PrMn_2O_5$ orders antiferromagnetically with $T_N = 25$ K, in agreement with previous susceptibility measurements [6]. In the temperature interval 18 K $< T <$ 25 K, the magnetic structure is defined by the propagation vector $\mathbf{k}_1 = (1/2, 0, 0)$, which implies a commensurate magnetic unit cell $(2a, b, c)$. In contrast, below 18 K two magnetic phases seem to exist, one of them defined by the propagation vector $\mathbf{k}_1 = (1/2, 0, 0)$ and the second one by $\mathbf{k}_2 = (0, 0, 1/2)$. In this second magnetic phase the magnetic cell would be $(a, b, 2c)$. At $T = 1.5$ K, for the magnetic phase associated with $\mathbf{k}_1$, the magnetic moments of the Mn atoms at sites 4h and 4f are 1.82(7) and 1.81(6) μ_B, respectively; for the magnetic phase associated with $\mathbf{k}_2$, the magnetic moments for the Mn(4h) and Mn(4f) are 0.59(5) and 2.62(5) μ_B, respectively. A strong reduction of the ordered magnetic moments with respect to the expected magnitudes (4 μ_B for Mn^{3+}, $t_{2g}^3e_g^1$; and 3 μ_B for Mn^{4+}, $t_{2g}^3e_g^0$) has frequently been observed in other oxides of the RMn_2O_5 series; for instance in $LaMn_2O_5$ at $T = 3.5$ K [15] the magnetic moments are 2.59(4) and 1.61(7) μ_B for Mn^{3+} (4h site) and Mn^{4+} ions (4f site), respectively. This reduction has been attributed to covalence effects.

In principle, it is expected that the magnetic moment of the Mn(4h) atoms at the pyramidal sites is greater than that of the Mn(4f) at the octahedral positions. The present results show that, in the magnetic phase associated with $\mathbf{k}_1$, the magnetic moments of the Mn^{3+} and Mn^{4+} ions are similar, and for the magnetic phase associated with $\mathbf{k}_2$, the magnetic moment of Mn^{3+} is smaller than that of Mn^{4+}. In fact the value of the magnetic moment of the Mn^{3+} ions is very small, 0.59(5) μ_B, and remains nearly constant across all the temperature range (figure 7). This last result could indicate that the contribution of the Mn atoms at site 4f is greater than that of the 4h site. On the other hand, the values of the magnetic moments of the Mn atoms in both magnetic phases have been determined by assuming that the proportions of both phases are the same (50% of each), which might not be the situation in $PrMn_2O_5$. This point could only be checked in a neutron diffraction experiment on a single crystal and under a magnetic field, preferentially enhancing one of the magnetic arrangements. This would also allow one confirm whether there are two independent $\mathbf{k}_1$ and $\mathbf{k}_2$ magnetic domains in the magnetic structure. In any case, the existence of two independent magnetic domains is something unexpected, so it implies that in both domains the magnetic energy is minimized and this happens for different $\mathbf{k}$ vectors. This could be due to the existence of some phase segregation. Effectively, the existence of some microstrain was determined in the sample, which could originate this phase segregation.

The crystallographic structure of the RMn_2O_5 compounds consists of chains of edge-sharing $Mn^{4+}O_6$ octahedron arranged along the c axis (figure 3). The different octahedral chains are interconnected by $Mn^{3+}O_5$ polyhedra. Two $Mn^{3+}O_5$ polyhedra form a dimer, constituted by two pyramidal units which are related by an inversion center. For the $\mathbf{k}_1$-domain, according to figure 5, the coupling of the magnetic moments of the Mn^{4+}ions of the octahedron along the c axis is ferromagnetic. However, for the $\mathbf{k}_2$-domain, as $\mathbf{k}_2 = (0, 0, 1/2)$ in the magnetic unit cell the coupling is $+--+$; this sequence is repeated along the c-axis. Therefore for the $\mathbf{k}_1$-domain the exchange interactions between the Mn^{4+} ions along the c axis are ferromagnetic, and for the $\mathbf{k}_2$-domain there are both ferromagnetic and antiferromagnetic exchange interactions. As regards the coupling between the two Mn^{3+} ions that constitute the dimer, in both the $\mathbf{k}_1$- and $\mathbf{k}_2$-domains the magnetic moments are antiferromagnetically coupled. This also happens for all the compounds of the RMn_2O_5 series.

One important difference found between the magnetic structures of the $\mathbf{k}_1$- and $\mathbf{k}_2$-domains concerns the orientation of the magnetic moments. For the $\mathbf{k}_1$-domain all the magnetic moments are oriented along the a axis. However,

for the $\mathbf{k}_2$-domain, the magnetic moments of the Mn^{4+} ions are oriented in the *ab* plane whereas the magnetic moments of the Mn^{3+} sublattice are directed along the *c* axis. This magnetic arrangement is reminiscent of that observed for $LaMn_2O_5$ [15]. In this compound the magnetic structure is commensurate with $\mathbf{k} = (0, 0, 1/2)$, and the magnetic moments of the Mn^{4+} ions are arranged along the *c* direction, whereas for the Mn^{3+} ions the moments are oriented in the *ab* plane. However, whereas in $LaMn_2O_5$ the couplings along the chains of Mn^{4+} octahedra are alternately AFM and FM (C_z mode), in $PrMn_2O_5$ a perfectly antiferromagnetic coupling is observed along the *c* axis (G_z mode). It is also worth comparing the magnetic structure of $PrMn_2O_5$ with those found for other members of the RMn_2O_5 family. Most of the RMn_2O_5 oxides exhibit a magnetic structure defined by the propagation vector $\mathbf{k} = (1/2, 0, \tau)$, except for $BiMn_2O_5$ with $\mathbf{k} = (1/2, 0, 1/2)$, $LaMn_2O_5$ with $\mathbf{k} = (0, 0, 1/2)$ and $DyMn_2O_5$ with $\mathbf{k}_1 = (1/2, 0, \tau)$ and $\mathbf{k}_2 = (1/2, 0, 1/2)$. Thus, for all of them the magnetic structure antiferromagnetically propagates along the *a* direction (excepting $LaMn_2O_5$); in $PrMn_2O_5$ the $\mathbf{k}_1$-domain also exhibits an antiferromagnetic propagation along *a*. Concerning the magnetic moment orientation, in $LaMn_2O_5$ and $PrMn_2O_5$ the moments of the Mn^{4+} ions are parallel to the *c* direction whereas for the rest of the compounds of the series the moments are in the (a, b) plane. This is related to the symmetry of the $Mn^{4+}O_6$ octahedra [15]. The Mn–O distances are more different as the R^{3+} ionic radius increases [6], so that higher symmetry of the octahedra is found for $LaMn_2O_5$ and $PrMn_2O_5$. Within the dimer units of the $Mn^{3+}O_5$ pyramids, the two Mn^{3+} spins also show an AFM coupling, with the magnetic moments lying on the *ab* plane for both $\mathbf{k}_1$- and $\mathbf{k}_2$-domains, as observed in $LaMn_2O_5$, the magnetic structure of which seems to be closely related to that of the present compound.

5. Conclusions

Specific heat and neutron diffraction measurements have confirmed that $PrMn_2O_5$ undergoes an onset of antiferromagnetic ordering below $T_N \approx 25$ K. However, analysis of the powder neutron diffraction patterns has shown that in the temperature range 18 K $< T <$ 25 K the magnetic structure is defined by $\mathbf{k}_1 = (1/2, 0, 0)$, and below 18 K the magnetic order is defined by the propagation vectors $\mathbf{k}_1 = (1/2, 0, 0)$ and $\mathbf{k}_2 = (0, 0, 1/2)$. Below 18 K two independent magnetic domains exist, with magnetic ordering given by $\mathbf{k}_1$ and $\mathbf{k}_2$. The Mn(4h) and Mn(4f) atoms contribute to both magnetic domains. The orientation of the moments of the Mn atoms is different for the two $\mathbf{k}_i$-domains. For the $\mathbf{k}_1$-domain all the magnetic moments are oriented along the *a* axis. Conversely, for the $\mathbf{k}_2$-domain the magnetic moments of the Mn^{4+} ions are orientated in the (a, b) plane whereas the magnetic moments of the Mn^{3+} sublattice are directed along the *c* axis. At $T = 1.5$ K, for the magnetic phase associated with $\mathbf{k}_1$, the magnetic moments of the Mn atoms at sites 4h and 4f are 1.82(7) and 1.81(6) μ_B, respectively; for the magnetic phase associated with $\mathbf{k}_2$, the magnetic moments for the Mn(4h) and Mn(4f) are 0.59(5) and 2.62(5) μ_B, respectively. Therefore, a strong reduction of the ordered magnetic moments is observed with respect to the expected magnitudes (4 μ_B for Mn^{3+}, $t_{2g}^3 e_g^1$; 3 μ_B for Mn^{4+}, $t_{2g}^3 e_g^0$) as has been frequently observed in other oxides of the RMn_2O_5 series. This reduction has been attributed to covalence effects.

Acknowledgments

We acknowledge the financial support of the Spanish Ministry of Science and Innovation to the project MAT2010-16404. We are grateful to the laboratory Leon Brillouin in Saclay (France) for making the neutron beam time available.

References

[1] Kimura T, Goto T, Shintani H, Ishizaka K, Arima T and Tokura Y 2003 *Nature* **426** 55
[2] Goto T, Kimura T, Lawes G, Ramírez A P and Tokura Y 2004 *Phys. Rev. Lett.* **92** 257201
[3] Hur H, Park S, Sharma P A, Ahn J, Guha S and Cheong S-W 2004 *Nature* **429** 392
[4] Quezel-Ambrunaz S, Bertau E F and Buisson G 1964 *C. R. Acad. Sci. Paris* **258** 3025
[5] Bertaut E F, Buisson G, Durif A, Mareschal A, Montmory M C and Quezel-Ambrunaz S 1965 *Bull. Soc. Chim. Fr.* **1132**
[6] Alonso J A, Casais M T, Martínez-Lope M J, Martínez J L and Fernández-Díaz M T 1997 *J. Phys.: Condens. Matter* **9** 8515–26
[7] Alonso J A, Casais M T, Martínez-Lope M J and Resines I 1997 *J. Solid State Chem.* **129** 105–12
[8] Kagomiya I, Kohn K and Uchiyama T 2002 *Ferroelectrics* **280** 131
[9] Inomata A and Kohn K 1996 *J. Phys.: Condens. Matter* **8** 2673
[10] Buisson G 1973 *Phys. Status Solidi* a **16** 533
[11] Buisson G 1973 *Phys. Status Solidi* a **17** 191
[12] Gardner P P, Wilkinson C, Forsyth J B and Wanklyn B M 1988 *J. Phys. C: Solid State Phys.* **21** 5653–61
[13] Bertaut E F, Buisson G, Quezel-Ambrunaz S and Quezel G 1967 *Solid State Commun.* **5** 25–30
[14] Muñoz A, Alonso J A, Casais M T, Martínez-Lope M J, Martínez J L and Fernández-Díaz M T 2002 *Phys. Rev.* B **65** 144423
[15] Muñoz A, Alonso J A, Casais M T, Martínez-Lope M J, Martínez J L and Fernández-Díaz M T 2005 *Eur. J. Inorg. Chem.* **2005** 685–91
[16] Blake G R, Chapon L C, Radaelli P G, Park S, Hur N, Cheong S-W and Rodríguez-Carvajal J 2005 *Phys. Rev.* B **71** 214402
[17] Wilkinson C, Sinclair F, Gardner P P, Forsyth J B and Wanklyn B M 1981 *J. Phys. C: Solid State Phys.* **14** 1671
[18] Tsujino H, Tanaka Y and Kohn K 1992 *Proc. 6th Int. Conf. on Ferrites (Tokyo and Kyoto)* ed M Abe and T Yamaguchi,
[19] Saito K and Kohn K 1995 *J. Phys.: Condens. Matter* **7** 2855–63
[20] Kobayashi S, Osawa T, Kimura H, Noda Y, Kagomiya I and Kohn K 2004 *J. Phys. Soc. Japan* **73** 1031
[21] Kobayashi S, Osawa T, Kimura H, Noda Y, Kagomiya I and Kohn K 2004 *J. Phys. Soc. Japan* **73** 1593
[22] Kobayashi S, Kimura H, Noda Y and Kohn K 2005 *J. Phys. Soc. Japan* **74** 468–72
[23] Higashiyama D, Miyasaka S and Tokura Y 2005 *Phys. Rev.* B **72** 064421
[24] Rietveld H M 1969 *J. Appl. Crystallogr.* **2** 65

[25] Rodríguez-Carvajal J 1993 *Physica* B **192** 55
[26] Bertaut E F 1963 *Magnetism* vol 3, ed G T Rado and H Shul (New York: Academic) chapter 4
[27] Schobinger-Papamantellos P, Rodríguez-Carvajal J, Prokes K and Buschow K H J 1996 *J. Phys.: Condens. Matter* **8** 8635–51
[28] Morozkin A V, Isnard O, Henry P and Manfrinetti P 2008 *J. Alloys Compounds* **464** 219–26
[29] García Soldevilla J, Blanco J A, Rodríguez Fernández J, Espeso J I, Gómez Sal J C, Fernández-Díaz M T, Rodríguez-Carvajal J and Paccard D 2004 *Phys. Rev.* B **70** 22411
[30] Laffargue D, Bourée F, Chevalier B, Roisnel T and Bordéré S 1998 *J. Alloys Compounds* **271–273** 444–7
[31] Heid C, Weitzel H, Bourdarot F, Calemczuk R, Vogt T and Fuers H 1996 *J. Phys.: Condens. Matter* **8** 10609–25
[32] King G, Wills A S and Woodward P M 2009 *Phys. Rev.* B **79** 224428
[33] Popa N C and Balzar D 2001 *J. Appl. Crystallogr.* **34** 187
[34] Caglioti G, Paleoti A and Ricci F P 1958 *Nucl. Instrum. Methods* **3** 223–6
[35] Fajar A, Gaunawan E, Kartini E, Mugirahardjo H and Ihsan M 2010 *Atom Indones.* **36** 111–5
[36] Martínez-Blanco D, Gorria P, Blanco J A, Pérez M J and Campo J 2008 *J. Phys.: Condens. Matter* **20** 335213